EXPLICIT MODELLING OF FIBRE PULLOUT IN CEMENTITIOUS COMPOSITES

***†Hui Zhang[1], Rena C. Yu[2], Shilang Xu[1]**

[1]College of Civil Engineering and Architecture, Zhejiang University, 310058, China.
[2]School of Civil Engineering, University of Castilla-La Mancha, Ciudad Real, Spain

*Presenting author: huizhangzju@zju.edu.cn
†Corresponding author: huizhangzju@zju.edu.cn

Abstract

It is well-known that fibres improve the performance of cementitious composites by acting as bridging ligaments in cracks. Such bridging behaviour is often studied through the fibre pullout tests. The relation between the pullout force versus slip end displacement is characteristic of the fibre-matrix interface. However, such a relation varies significantly with the fibre inclination angle. In the current work, we establish a numerical model to explicitly represent the fibre, matrix and the interface for arbitrary fibre orientations. Cohesive elements endorsed with mixed-mode fracture capacities are implemented to represent the bond-slip behaviour at the interface. Contact elements with Coulomb's friction are placed at the interface to simulate frictional contact. Matrix spalling is modelled through material erosion. The bond-slip behaviour is first calibrated through pull-out curves for fibres aligned with loading direction, then validated against experimental results carried out by Leung and Shapiro in 1999 for steel fibres oriented at 30° and 60°. The proposed methodology provides the necessary pull-out curves for a fibre oriented at a given angle for multi-scale models to study fracture in fibre-reinforced cementitious materials.

Keywords: Fibre-reinforced concrete, Pullout response, Cohesive model, Matrix spalling,

Introduction

Cementitious materials, known as a quasibrittle, have almost no ductility, additionally, have very low tensile strength. The addition of fibers in a cement-based matrix enables a considerable amount of energy dissipated during structural cracking.

The effectiveness of force transmission of certain fibres is often assessed by a pullout test, in which the force required to pull a fibre out of the hardened concrete is measured. This force is derived from interfacial bond, defined as the shear stress at the interface between the fibre and the surrounding matrix [1]–[4].

Classical approaches assume that the perfect bond on the interface between fibre and matrix will be maintained unless a failure criterion is achieved [5]. Stress criterion [6][7] or energy criterion [5][8][9] have been adopted, as well as cohesive approaches where bond stress is determined by relative slip between fibre and matrix [2][5][10][11]. Naaman et al. [2] indicated that for aligned fibres whose load direction is along the fibre direction, there are two types of shear bond at the interface: the elastic shear bond and the frictional one. If the elastic one exceeds the bond strength of the interface, bond becomes frictional in nature.

Based on the interfacial properties, Chanvillard [12] took into consideration the different phenomena existed in a non-straight fibre with a new micro-mechanical model. Ellis [13] carried out a simulation with emphasis of fibre morphology. Despite of the good agreement, only aligned fibres were considered in these two models.

In fibre reinforced cementitious material, most fibres lie at an angle to the load direction. For inclined fibres, besides bond strength and friction along the interface, additional phenomena such as fibre bending, matrix spalling and local friction effects need to be considered [14]–[17]. Furthermore, these micro-mechanisms are sensitive to fibre inclination angle and fibre material properties [3][9][14][15][16][18][19]. Fibre bending contributes increasingly more for larger inclination angles and the fibre curvature has an impact on the pressure distribution against the surrounding matrix. Because of the fibre curvature and residual stress at the interface, matrix is likely to crack and spall [14][16][19], which in turn influences the effective embedment length and deformation within the fibre.

A great deal of efforts have been put to study the above phenomena in the pullout process of inclined fibres. For example, Mortons and Groves [20] calculated the force needed to produce a plastic hinge in the fibre based on an elementary beam theory. The model reproduced well the experimental observations for lower inclination angles, but failed to do so for steep inclinations due to the fact that matrix spalling was not accounted for. Regarding the fibre as a beam bent on an elastic foundation with variable stiffness, Leung and Li [9] studied the coupled fibre bending-matrix spalling mechanism in random brittle fibre-reinforced brittle matrix composites. Afterwards, the micro-mechanical model was extended to ductile fibres [21]. However, the whole pullout curve was not simulated.

More comprehensive models such as Cailleux et al. [19] and Fantilli et al. [11], require a number of parameters which can only be obtained through pullout experiments in aligned as well as inclined fibres, and the numerical iterative procedures involved are tedious.

In spite of continuous efforts during the last decades, models that cover all the aforementioned phenomena, however, have been seldom developed to explicitly consider the whole pullout process for fibres at a random inclination angle. In this study, we endeavour to do so. Cohesive models able to represent mixed-mode fracture and Coulomb's friction at the interface between fibre and matrix are employed. In addition, fibre bending and matrix spalling are naturally taken into account owing to the explicit representation of the fibre, the matrix and the interface in between.

The paper is structured as follows. Section 2 describes the interfacial bond characteristics and matrix spalling. Afterwards, model calibration and validation are given in Section 3. The numerical results and relevant conclusions are respectively presented in Section 4 and Section 5.

Bond characterisation and matrix spalling

In this section, two major factors that determine the pullout response of a fibre with arbitrary orientation are explained in detail: bond characterisation and quantification of matrix spalling.

Interface bond characterisation

As a constitutive property of the interface, the shear stress versus slip relationship is very important for predicting both the mechanical and fracture properties of fibre reinforced composites. Naaman et al. [1] ascribed the presence and combination of four bond components: physical and chemical adhesion, the mechanical contribution of deformed or hooked fibres, the entanglement of fibres and friction. In this work, the concept of internal friction is illustrated and quantified through fitting with the test data of Leung and Shapiro [16].

Regardless of the fibre orientation, after debonding during pulling out, there exists certain frictional resistance which is mainly determined by the surface roughness. This component is denominated as internal fraction resis tance, τ_0. As for inclined fibres, pullout load is decomposed of a parallel force and a perpendicular force. The former pulls the fibre out while the latter bends the fibre and changes the direction of fibre during the pullout process. A constitutive law involving three constituents to govern the interface evolution is proposed as follows

$$\tau(\theta,s)=\tau_f(s)+\tau_b(s)+\mu p(\theta) \tag{1}$$

where μ is the friction coefficient of Coulomb, $p(\theta)$ is the pressure against the matrix when the fibre is inclined at an angle θ with respect to the external load direction. The first term, $\tau_f(s)$, is contributed by the internal friction, acting as a resistance between the fibre and the matrix. The second term, $\tau_b(s)$, represents the interfacial bonding caused by internal physical and chemical cohesion. The third term describes the shear stress due to dry friction, which works only when the fibre is oriented at a non-zero angle.

Authors are responsible for obtaining permission for reprinting any material included in their papers that is already copyrighted elsewhere.

In the case of constant friction, see Fig. 1, $\tau_f(s)$ is unchanging with the slip displacement s. In the current work, both $\tau_f(s)$ and $\tau_b(s)$ are decaying functions of s and they are assumed as linear-decreasing:

$$\tau_f(s)=\tau_0\left(1-\frac{s}{s_0}\right) \tag{2}$$

$$\tau_b(s)=(\tau_{\max}-\tau_0)\left(1-\frac{s}{s_c}\right) \tag{3}$$

where τ_0 represents the internal frictional resistance, τ_{max} is the bond strength, defined as the maximum shear stress resisted at the interface, covering both the internal bond and internal friction.

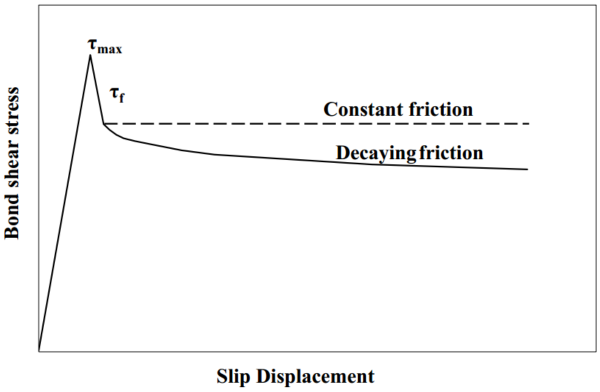

Figure 1. Interface bonding.

Eqs. (1-3) presents a gradual failure at the interface which is of vital importance, since in most actual fibre applications, the slip displacement is less than 1 mm, see Yu et al. [22]. When working in a corrosive environment, the maximum allowed crack opening in steel-fibre reinforced composites is 0.3 mm making it paramount to trait the detailed failure process at small slips.

Matrix spalling

The local curvature and stretching of the fibre segment at the free end will inevitably lead to spalling of matrix. Because the failure process starts near the interface within a narrow band, convergence problems led by excessive mesh distortion impedes the further modelling of the entire pullout process. As a result, simplifications are often assumed so that the spalling part is removed once the matrix tensile strength is reached [17][19][23][24]. The length of the eroded matrix along the fibre direction is the so-called spalling length, denoted as L_{sp}. The spalling length of the matrix can be estimated according to Laranjeira et al. [23] as follows:

$$aL_{sp}^2 + bL_{sp} + c = 0 \tag{4}$$

where

$$a=\frac{\sqrt{2}}{\sin\theta}+\frac{\cos\theta}{\sin^2\theta}, b=\frac{d_f}{\sin\theta}, c=-\frac{P_{\max}\sin\theta}{f_t} \tag{5}$$

in which, d_f is the fibre diameter, θ is the inclination angle, P_{max} is the peak pullout load of the aligned fibre. The results from Eq. (4) closely match the ones measured by scanning electron microscopy (SEM) by Leung and Shapiro [16].

In this work, Eq. (4) serves as a first approximation to obtain the size of the matrix wedge to be spalled off. Then trial runs are conducted to determine the moment to deactivate the matrix wedge. Then the elements within the matrix wedge stop to contribute to the overall stiffness and state variables. Furthermore, the first principal stress within the matrix is checked and the spalled length is adjusted if necessary.

Model calibration and validation

To explicitly model the physical phenomena in the pullout process, matrix is represented as solid elements with elastic constitutive law while fibre is by solid elements with bilinear kinematic plastic constitutive law. Cohesive elements representing mixed-mode fracture [25]-[29] are employed as the interface in between. Furthermore, contact pairs coincident with the cohesive elements are implemented to model friction after de-bonding.

Experimental setup of Leung and Shapiro,1999

To assess the effect of fibre yield strength on the maximum crack bridging force and total energy absorption, Leung and Shapiro [16] performed pullout tests for steel fibres of different yield strengths. All the fibres are of 0.5 mm in diameter and 22 mm in length. The pullout specimens are blocks of 25.4 mm× 12.7 mm × 9.5 mm in dimension, with effective embedment length of 10 mm. The material parameters of the matrix, fibre and the interface are given in Table 1, whereas the yield and tensile strengths of the four fibre types are listed in Table 2. Additionally listed in Table 2 is the critical fibre length, the maximum embedded length for a fibre to be pulled out from a matrix without rupture [14]. It is related with the maximum shear stress τ_{max} as follows

$$L_c = \frac{\pi d_f^2 / 4 f_y}{\pi d_f \tau_{\max}} = \frac{d_f f_y}{4\tau_{\max}} \tag{6}$$

Note that this estimation is for aligned fibres only, in the case of inclined ones, this length is smaller due to fibre bending.

Table 1. Material parameters for the matrix and the fibre given in [16].

	ρ [kg/m^3]	E [GPa]	υ -	f_c [MPa]
Matrix	2100	30	0.20	36.5$\pm$2.5
Steel fibre	7800	200	0.33	-

Table 2. Yield and tensile strength of the four types of fibres tested in [16], the corresponding L_c is listed for a diameter of 0.5 mm.

Fibre type	1	2	3	4
f_y [MPa]	275	469	635	954
f_t [MPa]	-	783	847	1023
L_c [mm]	12.7	21.7	29.4	44.2

Identification of the fibre-matrix interface properties

With the assumption that fibre-matrix interface property is uniform, the peak pullout load and maximum fictional load are respectively calculated as

$$P_{\max} = \pi d_f L_e \tau_{\max}, P_f = \pi d_f L_e \tau_0 \tag{7}$$

The values for P_{max} and P_f are determined from pullout response of aligned fibres, as shown in Fig. 2 and Fig. 3. The critical slip displacement for internal frictional resistance, s_0, is directly assumed as the final slip length, 9.0 mm approximately. The straight dotted line in Fig. 2a starts at the point (s_0, 0), follows the mean slope of the experimental curves and intercepts the load axis at (0, P_f). The values for P_{max} and P_f are averaged for the four types of fibres listed in Table 2 to obtain those of τ_{max} and τ_0 as well as their standard deviations in Table 3. The critical slip for interfacial bond, s_c, is determined through trial and error so that the first decaying branch of the numerical pullout responses, as demonstrated in Fig. 2b, should fall within the experimental range. As regards the friction coefficient given in Table 3, it is estimated according to the experimental results of Chanvillard [12], which was also adopted by Laranjeira et al. [17].

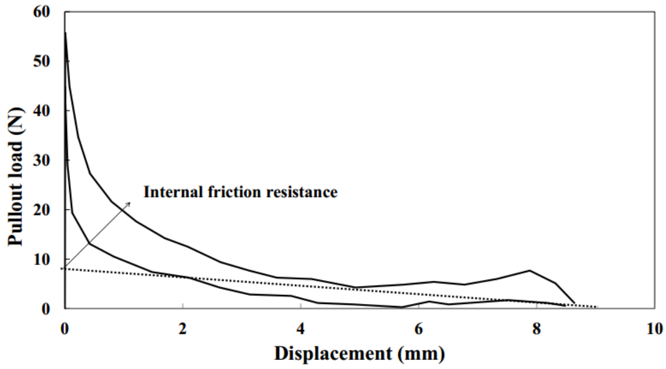

Figure 2. Experimental range for pullout curves for aligned fibre type 2 (yield strength 469 MPa) [16], where the dotted line represents the contribution from internal friction.

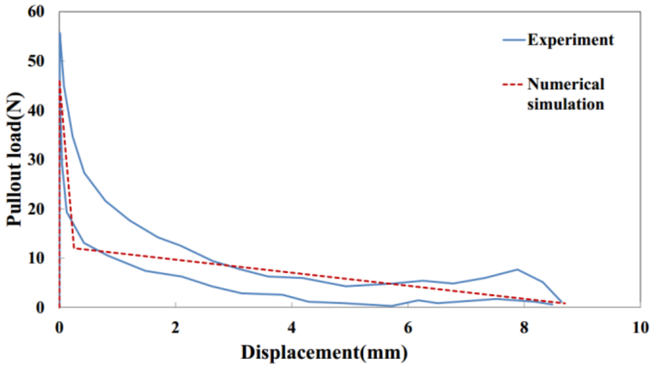

Figure 3. The corresponding numerical pullout curve plotted against the experimental range for aligned fibre type 2 (yield strength 469 MPa) [16].

Table 3. Extracted parameters of the fibre-matrix interface from the experimental data of Leung and Shapiro [16].

$\tau_{\max}$	τ_0	s_0	s_c	μ
[MPa]	[MPa]	[mm]	[mm]	-
2.7 ± 0.1	-	783	847	1023

Numerical model

Fig. 4 illustrates the in-plane dimensions and boundary conditions to simulate the pullout tests performed by Leung and Shapiro [16]. Note that within a two-dimensional plain stress framework, the fibre thickness, T_f, is calculated through Eq. (8) so that the contact area at the interface is the same as that of the tested one.

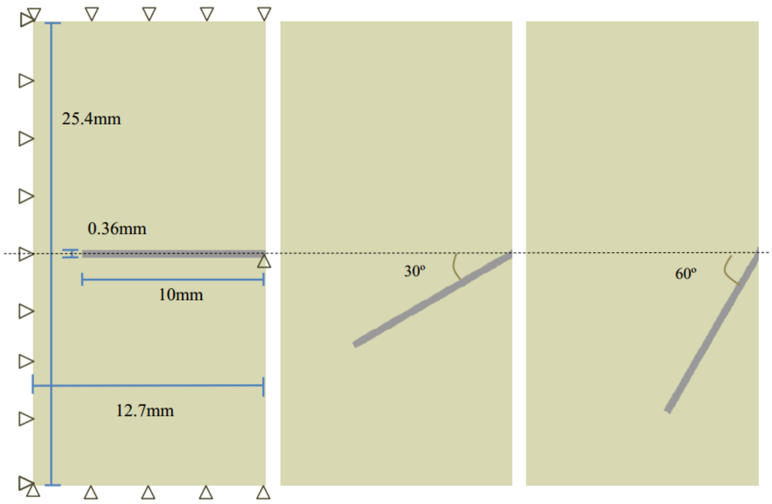

Figure 4. In-plane dimensions and boundary conditions for the pullout tests performed by Leung and Shapiro [16], with fibre inclination angle of 0°, 30° and 60°.

Similiarly, the fibre height, H_f, is determined via Eq. (9) so that the second moment of inertia is the same as the original fibre. For the case of fibre diameter of 0.5 mm, T_f and H_f are computed as 0.785 and 0.36 mm respectively.

$$T_f = \frac{\pi d_f L_f}{2L_f} \tag{8}$$

$$H_f = \left(\frac{\pi d_f^4 / 64}{T_f / 12} \right)^{1/3} \tag{9}$$

Boundary conditions are described in Fig. 4. Vertical displacements are prevented on the top and bottom sides, whereas horizontal movements are impeded on the left. The right end of the fibre is fixed in the vertical direction so that only horizontal movement is permitted. The pulling process is carried out with intervals of 0.001 mm in the horizontal direction until 0.3 mm, followed with increments of 0.01 mm until the end.

Mesh description

A typical mesh and detailed element distribution around the fibre for the inclination angle of 30° is demonstrated in Fig. 5. Note that the right end of fibre leans on a matrix wedge which will spall later on. For this particular case, the matrix and the fibre consist of 2198 and 154 solid elements respectively, whereas 289 contact pairs are placed at the interface. The mesh sensitivity analysis performed to achieve a balance between the computational efficiency and accuracy is going to be presented in Section 4.

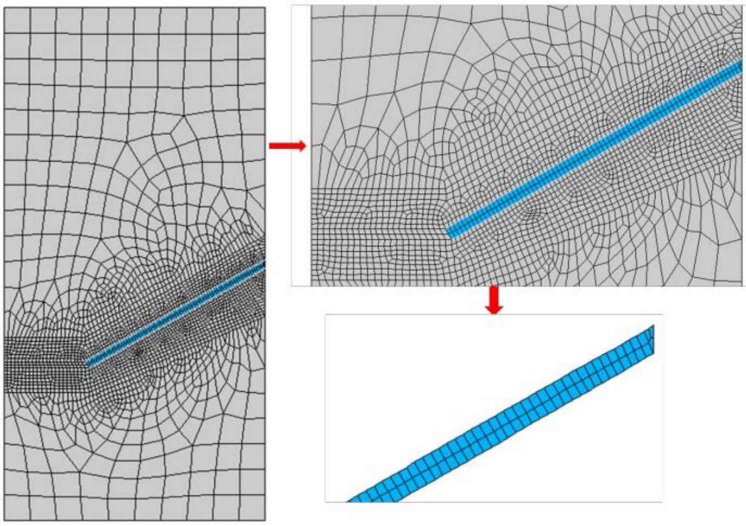

Figure 5. Typical mesh (left), zoomed in around the fibre (top right) and discretisation of the fibre (bottom right).

Numerical results and discussion

In this section, we first conduct the mesh sensitivity analysis along the fibre transverse and longitudinal directions to determine the particular mesh to employ for further studies. Second, the entire pullout load vs slip displacement curves are extracted to compare with those obtained experimentally by Leung and Shapiro [16]. Third, the von Mises stress and the first principle stress evolutions are explored both for the fibre and the matrix. Finally, the pullout work is obtained.

Mesh sensitivity analysis

The mesh-sensitivity analysis is carried out for the inclination angle of 30° and the yield strength of 635 MPa type 3 in Table 2). Two kinds of mesh sensitivities are studied: the refinement in the transverse direction and along axial direction of the fibre. The former is to check the capacity of the mesh in the fibre to bear bending moments, whereas the latter is to assess if the discretisation is fine enough to resolve the slip length.

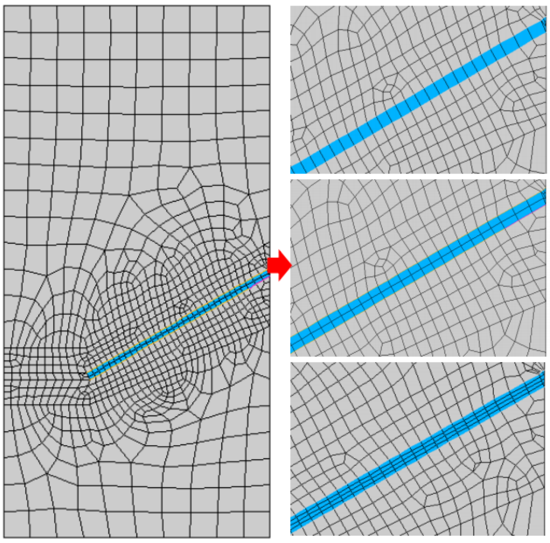

Figure 6. Different number of divisions in fibre transverse direction (one, two and four).

In the transverse direction, the fibre is split into one, two or four divisions, see Fig. 6, the corresponding load-displacement curves are plotted in Fig. 7. Meshes of two divisions across the transverse direction are employed for further studies. Along the longitudinal direction of the fibre, four different element sizes are considered: 0.303 mm, 0.222 mm, 0.135 mm and 0.068 mm, which lead to 33, 45, 74 and 148 divisions along the 10-mm length, see Fig. 8, the corresponding pullout load versus slip end displacement curves are depicted in Fig. 9. In order to keep a balance between the computational efficiency and accuracy of sought results, the mesh size of 0.135 mm is selected for further studies.

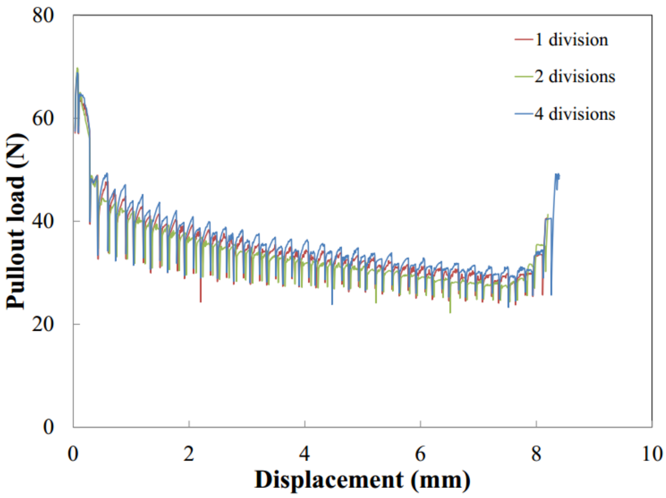

Figure 7. The pullout load vs displacement responses corresponding to different number of divisions in fibre transverse direction (one, two and four) .

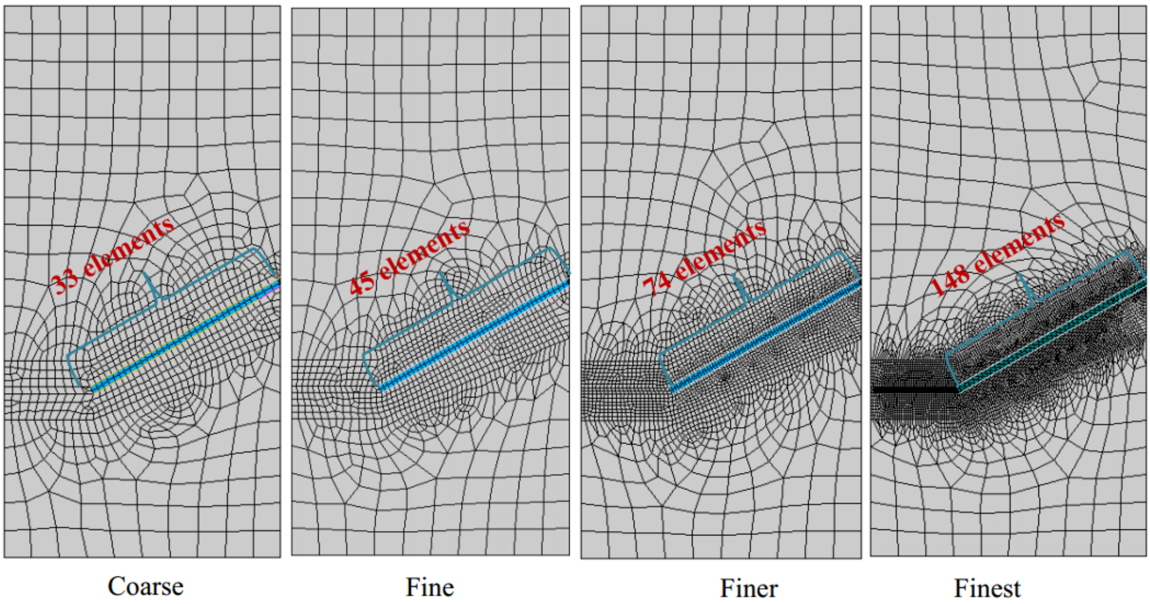

Figure 8. Different element sizes (number of divisions) along the fibre.

In addition, From Fig.9, it is observed that the maximum pullout load was achieved at slip displacement of 0.07 mm, this verifies the statement of Morton and Groves [20], who claimed that this value should be of the order of, but less than half a fibre diameter.

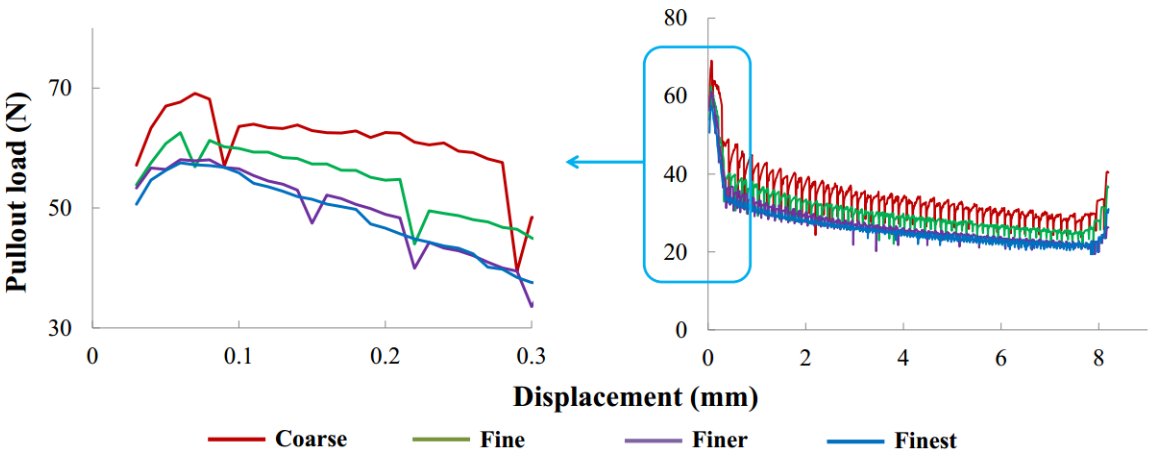

Figure 9. The pullout load-displacement responses corresponding to different element sizes (number of divisions) along the fibre.

Validation against experimental pullout load vs displacement response

In order to verify the previously developed methodology, we compare the entire pullout curves with their experimental counterparts given by Leung and Shapiro [16].
This comparison is displayed in Fig. 10 for fibres inclined at 30° and 60° with four different yield strengths given in Table 2. Note that both the peak loads and the general tendency are well captured, the numerical curves fall within the experimental range, in particular the rising tail at the end of each pullout process is also reproduced.

Stress evolution within the fibre

Taking fibre type 2 (yield strength 469 MPa) with inclination angle of 30° as an example, the von Mises stress evolution for several characteristic points within the fibre are examined. These points are the pullout end A, the embedded end D, two intermediate ones B (location of matrix spalling) and C, as depicted in Fig. 11. Note that at point A, the first peak stress was obtained when the pullout load reached its maximum due to interface debonding. Then after a slight decrease, this stress increased again until yielding at the slip end displacement of 3 mm. Similar peaks are observed for B and C at slip displacement of 0.3 mm and a second peak upon yielding at 2 mm for point B and 5 mm for point C respectively. The second peak is attributed to the stress concentration due to the cusp formed by matrix spalling. This is the snubbing effect introduced by Li et al. [14].

In Fig. 12 and Fig. 13, the first principal stress distributions in the fibre at different loading stages are plotted for type-2 fibre inclined at 30° and type-3 fibre inclined at 60° respectively. Note that during the pullout process, there are stress gradients both in the transversal direction and along the longitudinal one, which indicates bending contribution. Stress concentration is also observed at the fibre exit point. In addition, the maximum tensile stress is always inferior to the fibre tensile strength. This means that the fibre was pulled out but not broken.

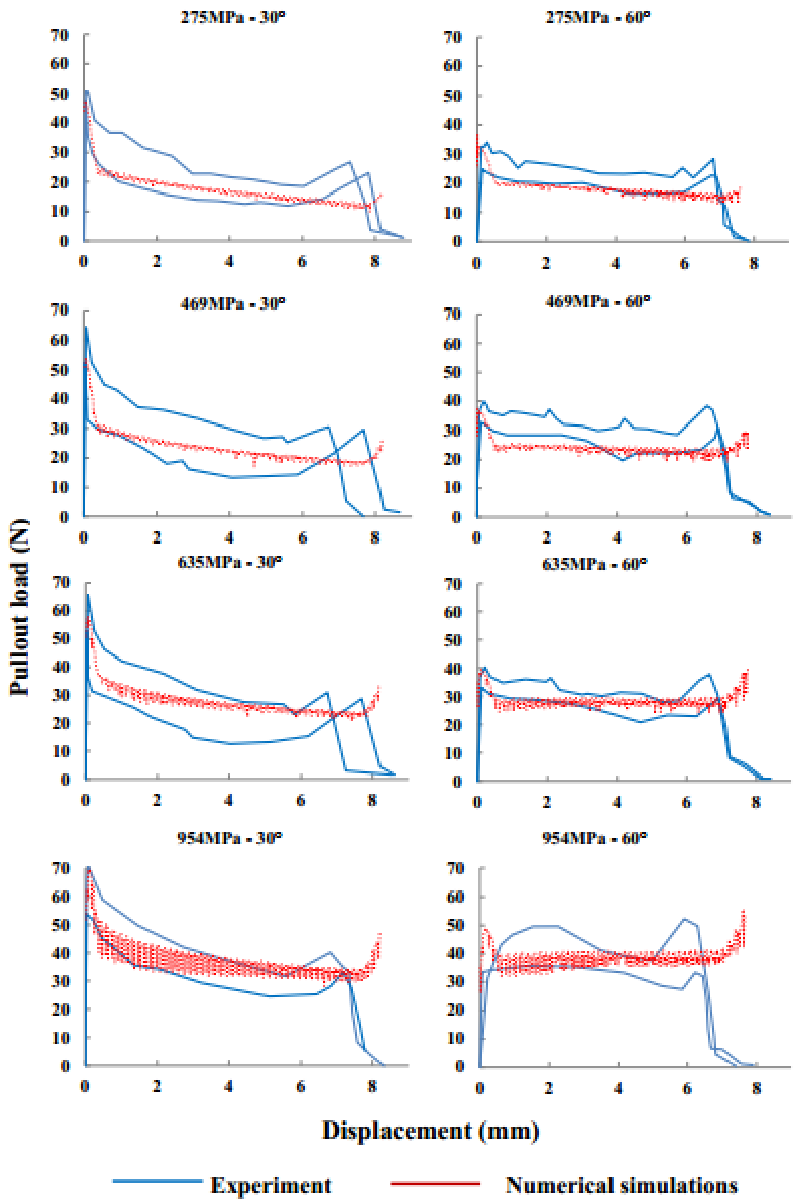

Figure 10. Numerical-experimental comparison: complete pullout curves for the four yield strengths given in Table 2, the fibre is inclined either at 30° (left column) or 60° (right column).

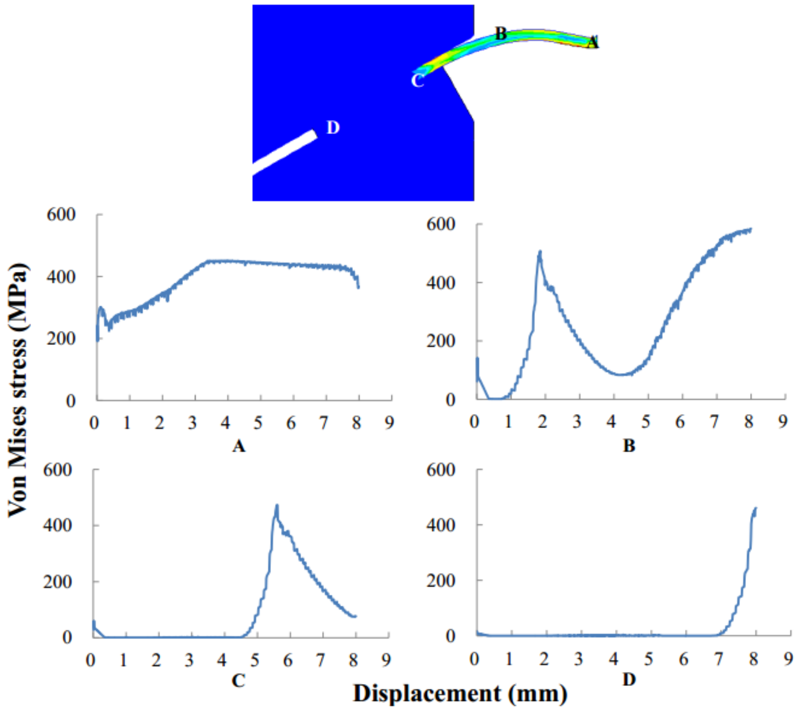

Figure 11. Four positions (A, B, C and D) within the fibre during pullout and the corresponding von Mises stress evolution for type 2 (fibre yield strength 469 MPa).

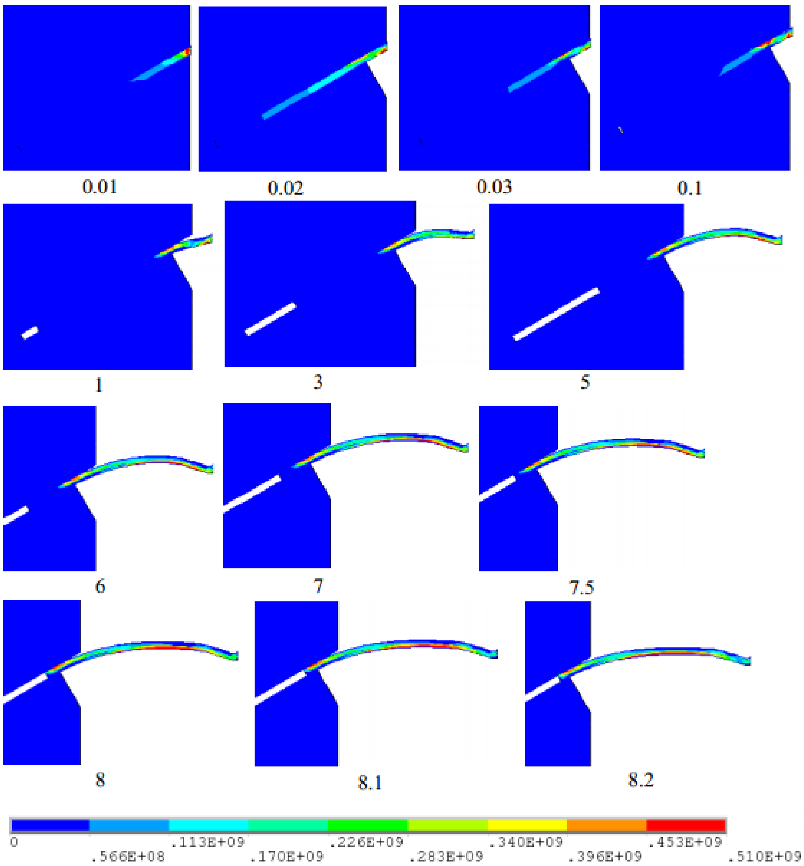

Figure 12. The first principle stress evolution (in Pa) for pullout displacement from 0.01 mm to 8.2 mm for fibre inclination of 30° and yield strength of 469 MPa (type 2 in Table 2).

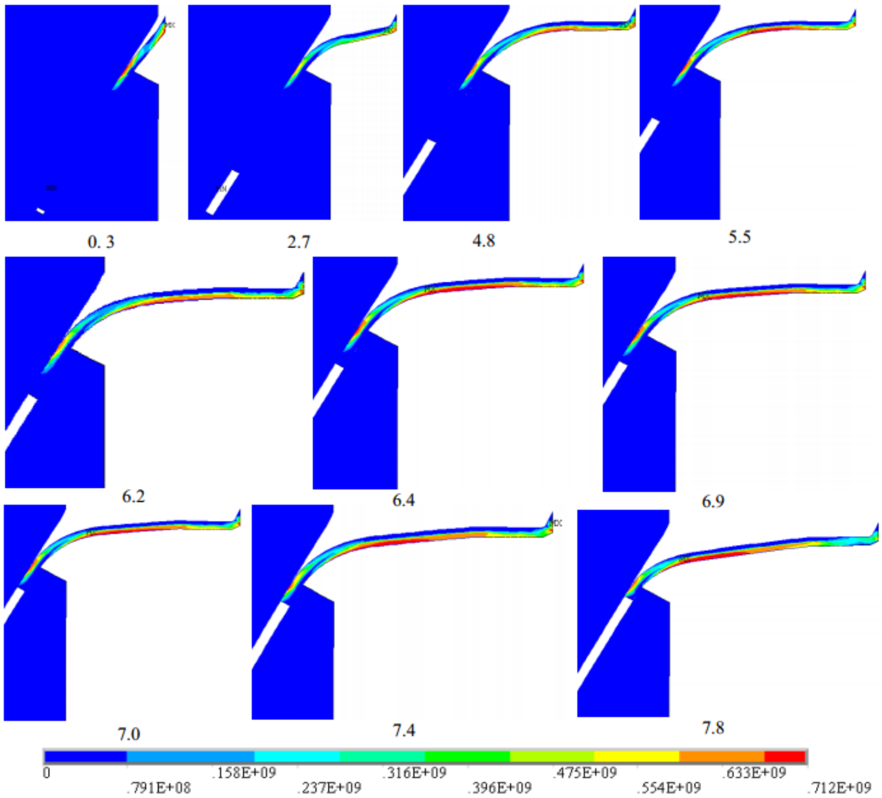

Figure 13. The first principle stress evolution (in Pa) for pullout displacement from 0.3 mm to 7.8 mm for fibre inclination of 60° and yield strength of 635 MPa (type 3 in Table 2).

Stress evolution in the matrix

For the matrix, we are more concerned on the tensile stress distribution to ensure that no fracture should take place where matrix spalling is not expected. Three representative points, E, F and G, see Fig. 14, are selected to display the first principal stress evolution in the matrix. The point E is where the matrix is expected to spall. The point G is the location where the fibre is anchored, whereas F is the point in the matrix close to the fibre centre.

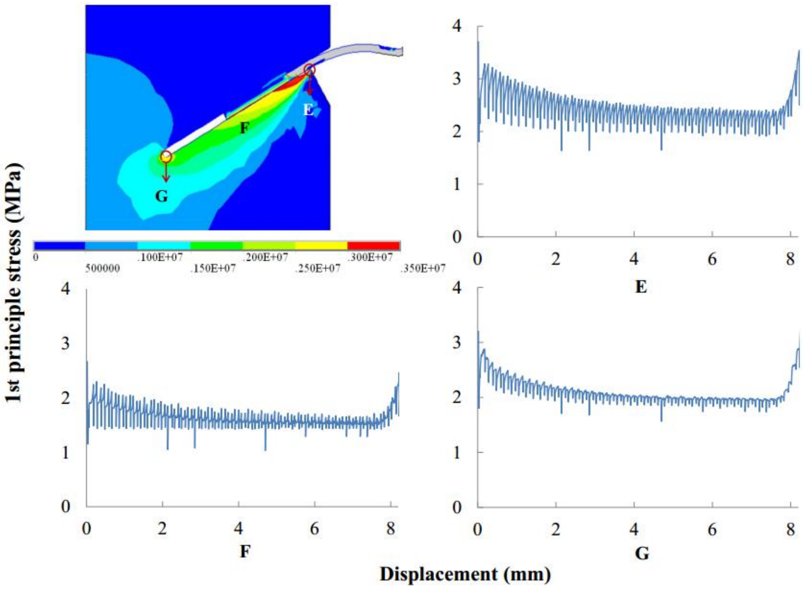

Figure 14. Three positions (E, F and G) in the matrix and the corresponding first principle stress evolution during pullout (the top left one is in Pa while the other three in MPa).

Since the tensile strength was not measured, we estimate it to be 1/12 of the compressive strength, which is 3.0 MPa. Note that at point E, there is significant stress fluctuation during the pullout process. This indicates, on the one hand, the stressing-relaxing cycle endured by the matrix. On the other hand, it can be attributed to the fact that the spalled matrix is assigned with a zero stiffness at the moment of spalling, whereas the real failure process is gradual. The stress evolution curves at points F and G, assimilate those of global pullout curves in Fig. 10, each with a different amplitude.

Furthermore, it is noted from Fig. 10 that the maximum tensile stress due to axial pull out of the fibre and bending load occurs at the close region at the fibre exit point. This confirms the assumption adopted by Zhang and Li [30] in their study on the effect of inclination angle on fibre rupture load in fibre reinforced cementitious composites.

Variation of the pullout work with respect to fibre yield strength

The pullout work is calculated as the area under the load vs slip displacement curve. In Fig. 15, both experimenta and numerical values for fibres inclined at 30° and 60° are depicted. Note that as a general trend, the pullout work increases with the increase of fibre yield strength, and such a tendency is correctly captured by our numerical model.

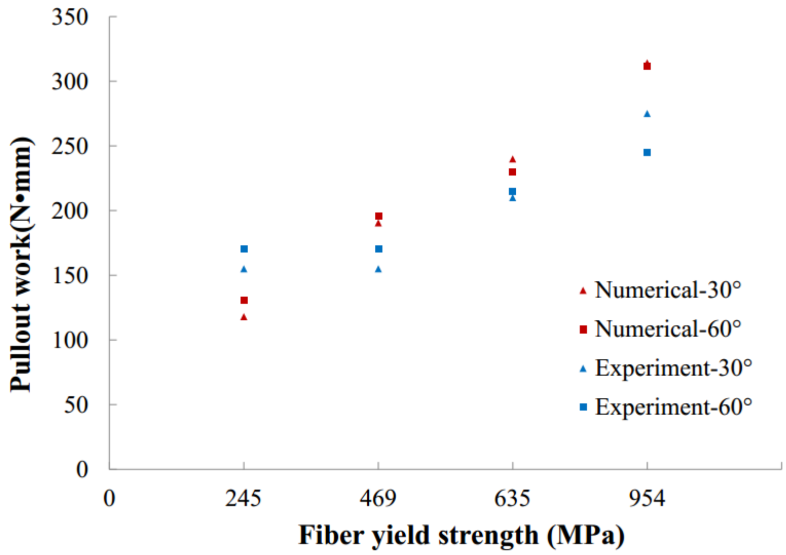

Figure 15. Pullout work vs fibre yield strength.

The maximum pullout load

To explore the effect of fibre inclination, a spectrum of angles up to 85° are simulated by keeping the fibre, matrix and interface properties fixed. It is known that the length of spalled matrix and the time when the matrix spalls both matter in the pullout responses. According to Laranjeira et al. [23], spalling is considered to take place just after the beginning of fibre debonding but prior to its full accomplishment. After some trial runs, this slip displacement is estimated, which is around 0.01 mm. Simulations of different fibre yield strengths are carried out and the obtained pullout curves are plotted in Fig. 16, the corresponding fitting parameters are given in Table 4.

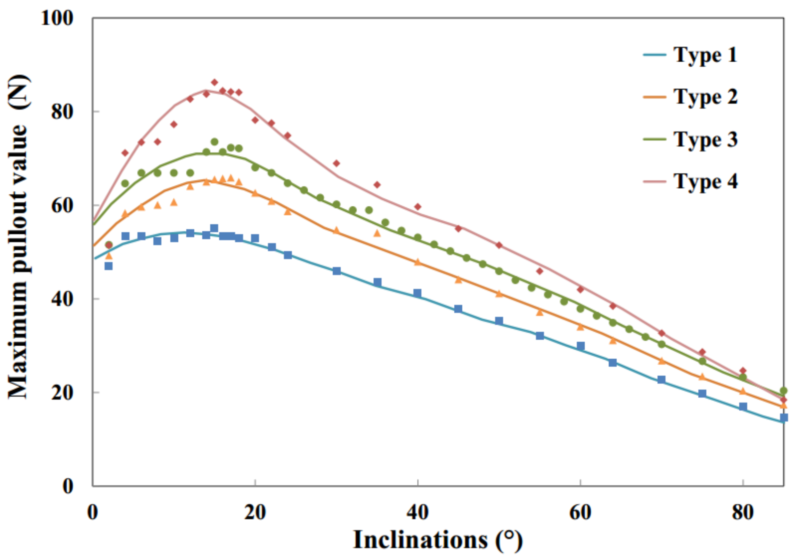

Figure 16. Maximum pullout load vs. inclination angle for the four yield strengths given in Table 2 and fitted curves using Eq. 10 with parameters given in Table 4.

$$P_{\max}(\theta) = F_1 \exp\left[-\left(\frac{\theta-\alpha_1}{\beta_1}\right)^2\right] + F_2 \exp\left[-\left(\frac{\theta-\alpha_2}{\beta_2}\right)^2\right] \tag{10}$$

Table 4. Fitted parameters for the maximum pullout load vs fibre inclination angle.

Fibre type	F_1 [N]	F_2 [N]	α_1 [°]	α_2 [°]	β_1 [°]	β_2 [°]
1	15.5	42.0	7.9	26.2	19.7	56.4
2	18.1	49.4	12.7	26.7	16.2	55.7
3	20.1	54.2	12.6	27.4	16.0	55.9
4	33.7	59.0	12.7	33.0	14.6	48.2

From Fig. 16, when the fibre is inclined at angles around 12° or 15°, the maximum pullout load is the largest. After that, the maximum pullout load goes down almost linearly. This differs from the result of Morton and Groves [20], who claimed that θmax is about 45° for polyester resin matrix of rather high tensile strength and steel fibres of high yield strength. This indicates that optimum inclination angle for maximum pullout resistance varies with both fibre and matrix strength as well as the interface properties.

CONCLUSIONS

We have proposed a numerical model to explicitly reproduce the pullout behaviour of a single fibre embedded within a cement-based matrix. This model takes into consideration of the gradual deterioration of interface bond, internal and dry friction as well as matrix spalling. In particular, a constitutive law which isolates the contributions of internal bond, internal friction and dry friction is formed and validated. Cohesive elements endorsed with mixed-mode fracture capacities are implemented to represent the bond-slip behaviour at the interface. Contact elements with Coulomb's friction are placed at the interface to simulate frictional contact. Matrix spalling is modelled through material erosion. The bond-slip behaviour is first calibrated through pull-out curves for fibres aligned with loading direction, then validated against experimental results carried out by Leung and Shapiro for steel fibres oriented at 30° and 60°. The influence of fibre yield strength on the stress distribution within the fibre and the matrix, the effect of the inclination angle on the pullout response are all explored in detail. The proposed methodology provides the necessary pull-out curves for a fibre oriented at a given angle for multi-scale models to study fracture in fibre-reinforced cementitious materials.

References

[1] Naaman, A. E., Namur, G., Najm, H., and Alwan, J. (1989). Bond Mechanisms in fibre reinforced cement-based composites. *Report UMCE 89-9*, Dept. of Civil Engineering, Univ. of Michigan, Ann Arbor, Michigan:1–233.

[2] Naaman, A. E., Namur, G., Alwan, J. M., and Najm, H. (1991). Fiber pullout and bond slip. I: Analytical study. *Journal of Structural Engineering*, **117**:2769–90.

[3] Banthia, N. and Trottier, J. (1994). Concrete reinforced with deformed steel fibers, part I: bond-slip mechanisms. *ACI Materials Journal*, **91**:435–446.

[4] Groth, P. (2000). *Fibre reinforced concrete fracture mechanics methods applied on self-compacting concrete and energetically modified binders*. PhD thesis, Lulea University of Technology, Sweden.

[5] Shah, S. P. and Ouyang, C. (1991). Mechanical-behavior of fiber-reinforced cement-based composites. *Journal of the American Ceramic Society*, **74**:2727–2953.

[6] Lawrence, P.(1972). Sometheoreticalconsiderationsoffiberpull-outfromanelasticmatrix. *Journal of Materials Science*, 7:1–6.

[7] Leung, C. K. Y. and Li, V. C. (1991). New strength-based model for the debonding of discontinuous fibers in an elastic matrix. *Journal of Materials Science*, **26**:5996–6010.

[8] Stang, H., Li, Z., and Shah, S. P. (1990). Pullout problem - stress versus fracture mechanical approach. *Journal of Engineering Mechanics-ASCE*, **116**:2136–2150.

[9] Leung, C. and Li, V. (1992). Effect of fiber inclination on crack bridging stress in brittle fiber reinforced brittle matrix composites. *Journal of the Mechanics and Physics of Solids*, **40**:1333–1362.

[10] Wang, Y., Li, V. C., and Backer, S. (1988). Modelling of fibre pull-out from a cement matrix. *International Journal of Cement Composites and Lightweight Concrete*, **10**:143–149.
[11] Fantilli, A. P. and Vallini, P. (2007). A cohesive interface model for the pullout of inclined steel fibers in cementitious matrixes. *Journal of Advanced Concrete Technology*, **5**:247–258.
[12] Chanvillard, G. (1999). Modeling the pullout of wire-drawn steel fibers. *Cement and Concrete Research*, **29**:1027–1037.
[13] Ellis, B., McDowell, D, L., and Zhou, M. (2014). Simulation of single fiber pullout response with account of fiber morphology. *Cement and Concrete Composites*, **48**:42–52.
[14] Li, V., Wang, Y., and Backer, S. (1990). Effect of inclining angle, bundling and surface treatment on synthetic fibre pull-out from a cement matrix. *Composites*, **21**:132–140.
[15] Ouyang, C., Pacios, A., and Shah, S. (1994). Pullout of inclined fibers from cementitious matrix. *Journal of Engineering Mechanics*, **120**:2641–2659.
[16] Leung, C. and Shapiro, N. (1999). Optimal steel fiber strength for reinforcement of cementitious materials. *Journal of Materials in Civil Engineering*, **11**:116–123.
[17] Laranjeira, F. (2011). *Design-oriented constitutive model for steel fiber reinforced concrete*. PhD thesis, Universitat Politècnica de Catalunya.
[18] Naaman, A. and Shah, S. (1976). Pull-out mechanism in steel fiber-reinforced concrete. *Journal of the Structural Division*, **102**(8):1537–1548.
[19] Cailleux, E., Cutard, T., and Bernhart, G. (2005). Pullout of steel fibres from a refractory castable: experiment and modelling. *Mechanics of materials*, **37**:427–445.
[20] Morton, J. and Groves, G. (1974). The cracking of composites consisting of discontinuous ductile fibres in a brittle matrix - effect of fibre orientation. *Journal of Materials Science*, **9**:1436–1445.
[21] Leung, C. and Chi, J. (1995). Crack-bridging force in random ductile fiber brittle matrix composites. *Journal of Engineering Mechanics*, **121**:1315–1324.
[22] Yu, R., Cifuentes, H., Rivero, I., Ruiz, G., and Zhang, X. (2016). Dynamic fracture behavior in fibre-reinforced cementitious composites. *Journal of the Mechanics and Physics of Solids*, pageDOI:10.1016/j.jmps.2015.12.025.
[23] Laranjeira, F., Aguado, A., and Molins, C. (2010). Predicting the pullout response of inclined straight steel fibers. *Materials and Structures*, **43**:875–895.
[24] Brandt, A. (1985). On the optimal direction of short metal fibres in brittle matrix composites. *Journal of Materials Science*, **20**:3831–3841.
[25] Camacho, G. and Ortiz, M. (1996). Computational modelling of impact damage in brittle materials. *International Journal of Solids and Structures*, **33** (20-22):2899–2938.
[26] Ruiz, G., Pandolfi, A., and Ortiz, M. (2001). Three-dimensional cohesive modeling of dynamic mixed-mode fracture. *International Journal for Numerical Methods in Engineering*, **52**(1-2):97–120.
[27] Alfano, G. and Crisfield, M. (2001). Finite element interface models for the delamination analysis of laminated composites: mechanical and computational issues. *International Journal for Numerical Methods in Engineering*, **50**:1701–1736.
[28] Yu, R. C. and Ruiz, G. (2006). Explicit finite element modeling of static crack propagation in reinforced concrete. *International Journal of Fracture*, **141**:357–372.
[29] Yu, R., Zhang, X., and Ruiz, G. (2008). Cohesive modeling of dynamic fracture in reinforced concrete. *Computers and Concrete*, **5**(4):389–400.
[30] Zhang, J. and Li, V. (2002). Effect of inclination angle on fiber rupture load in fiber reinforced cementitious composites. *Composites Science and Technology*, **62**:775–781.